JACS
JOURNAL OF THE AMERICAN CHEMICAL SOCIETY

Article

pubs.acs.org/JACS

Highly Ordered *n*/*p*-Co-assembled Materials with Remarkable Charge Mobilities

Javier López-Andarias,[†,⊥] María José Rodriguez,[‡,⊥] Carmen Atienza,[†,⊥] Juan Luis López,[†] Tsubasa Mikie,[§] Santiago Casado,[∥] Shu Seki,[§] José L. Carrascosa,*[,‡,∥] and Nazario Martín*[,†,∥]

[†]Departamento de Química Orgánica I, Facultad de Ciencias Química, Universidad Complutense, E-28040 Madrid, Spain

[‡]Centro Nacional de Biotecnología (CNB), CSIC, E-28049 Madrid, Spain

[§]Department of Applied Chemistry, Graduate School of Engineering, Osaka University, Osaka 565-0871, Japan

[∥]IMDEA-Nanoscience, Campus de Cantoblanco, E-28049 Madrid, Spain

Supporting Information

ABSTRACT: Controlling self-organization and morphology of chemical architectures is an essential challenge in the search for higher energy-conversion efficiencies in a variety of optoelectronic devices. Here, we report a highly ordered donor/acceptor functional material, which has been obtained using the principle of ionic self-assembly. Initially, an electron donor π-extended tetrathiafulvalene and an electron-acceptor perylene-bisimide were self-organized separately obtaining *n*- and *p*-nanofibers at the same scale. These complementary *n*- and *p*-nanofibers are endowed with ionic groups with opposite charges on their surfaces. The synergic interactions establish periodic alignments between both nanofibers resulting in a material with alternately segregated donor/acceptor nanodomains. Photoconductivity measurements show values for these *n*/*p*-co-assembled materials up to 0.8 $cm^2\ V^{-1}\ s^{-1}$, confirming the effectiveness in the design of these heterojunction structures. This easy methodology offers great possibilities to achieve highly ordered *n*/*p*-materials for potential applications in different areas such as optoelectonics and photovoltaics.

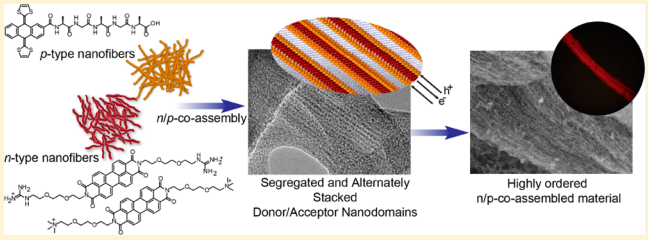

INTRODUCTION

The control on the organization and morphology of organic materials at different scales is an essential challenge in current science.[1] In particular, organic materials employed for obtaining efficient photovoltaic devices require a controlled segregation of electron donor/acceptor domains in the active layers because transport of the photogenerated charge carriers occurs through these domains to the electrodes. This control over the organization of nanostructured domains at the same length scale generally results in an increase in conductivity or photoconductivity values.[2] One of the approaches to prepare optoelectronic materials for photon-energy conversion is the use of covalent donor−acceptor (D-A) dyads. In this context, a great variety of D-A dyads have been reported with an elaborated synthetic strategy.[3−5] These D-A dyads provide nanoscale D-A heterojunctions with different morphologies such as fibrous,[3] tubular,[4] or liquid crystals, to name a few.[5]

On the other hand, supramolecular chemistry is gaining attention, when compared to covalent methodologies, due to its higher versatility and easier ensembles preparation. From small molecules and through weak and non-covalent intermolecular interactions such as hydrogen bonding, metal coordination, hydrophobic forces, van der Waals forces, $\pi-\pi$ stacking, and electrostatic interactions, it is possible to reach highly ordered structures at the nano and mesoscales.[6]

Here, we now report, to the best of our knowledge, the first example of highly ordered *n*/*p*-functional materials obtained by the electrostatic co-assembly of two complementary *n*- and *p*-nanofibers, which have been previously formed through self-assembled small molecules, namely a π-extended tetrathiafulvalene (exTTF) derivative as electron-donor and a perylene-bisimide (PBI) derivative as electron-acceptor (Figure 1). The only requirements for the electrostatic co-assembly were that (i) the *n*- and *p*-nanofibers should be endowed with ionic groups with opposite charges on their surfaces and (ii) these fibers should be of the same size. Our approach has important advantages with respect to that previously reported since it does not require neither tedious synthetic procedures nor special experimental conditions to obtain highly ordered materials. Moreover, our proposal design leads to the formation of *n*/*p*-co-assembled materials through the long-axis alignment of the fibers, which results in an improvement in charge-transport properties.

Recently, we have reported the formation of p-type nanofibers from a curved 9,10-di(1,3-dithiol-2-ylidene)-9,10-dihydroanthracene (exTTF) moiety which is covalently connected to a pentapeptide sequence (H_2N-AGAGA-COOH) with a carboxylic acid in the termini position.[7] The

Received: November 3, 2014
Published: December 21, 2014

DOI: 10.1021/ja510946c
J. Am. Chem. Soc. 2015, 137, 893−897

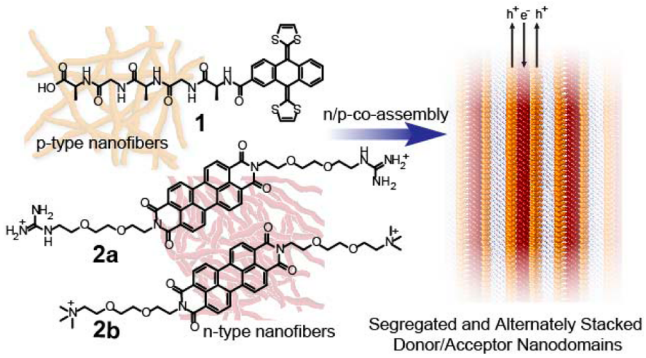

Figure 1. (Left) Molecular structures with schematic nanoarchitectures of exTTF derivative **1** and PBI derivatives **2a**,**b**. (Right) Schematic representation of the *n*/*p*-material obtained by the co-assembly of previously self-assembled molecules.

nanofiber formation was promoted by $\pi-\pi$ interaction between exTTF units and the β-sheet-forming peptide. The carboxylic acid groups not only guaranteed the water solubility, but also provided negative charges on the surface of fibers, which further enabled an external control to the aggregates by charge screening. By considering the above points, we have designed two different complementary acceptor moieties of PBI, which are symmetrically functionalized with polar tails to ensure the solubility in aqueous medium. Furthermore, guanidinium or quaternary ammonium groups (**2a**,**b**, respectively) present in the terminal positions of PBI were acting as counterions for the carboxylic acids in the complementary exTTFs arrays (for synthetic procedure see Supporting Information). Similar to *p*-type exTTF fibers, PBI was able to form self-assembled *n*-type nanofibers that will be described below.[8] The major challenge in this approach is the ionic co-assembly of the individually self-assembled nanofibers to form highly ordered *p*/*n*-functional materials, which guaranteed an enhancement in their photoconductivity properties and, thereby maximize their potential in, for instance, photovoltaic device applications (Figure 1).

RESULTS AND DISCUSSION

Self-Organization of PBI Molecules in Water. Initially, the ability of the PBI derivatives (**2a**,**b**) to form self-assembled architectures was examined by UV−vis spectroscopy and microscopic techniques. The absorption spectra of **2a**,**b** in methanol showed a well-resolved vibronic structure ranging from 400 to 500 nm which is characteristic for the S_0-S_1 transition of isolated PBI chromophore (Figure S1). However, the absorption spectra of **2a**,**b** in distilled water at different concentrations ($1 \times 10^{-5}-1 \times 10^{-3}$ M) showed a broad spectrum with a lower peak intensity and significant blue-shift in the absorption maximum (from 520 to 500 nm) with appearance of a shoulder peak at 542 nm. These features suggest the formation of face-to-face π stacks (H-aggregate) of rotationally displaced PBI chromophores. The morphology of these PBI aggregates (**2a**,**b**) dried from aqueous solution has also been studied using atomic force microscopy (AFM), and the images obtained are shown in Figure S2. The formation of fibers was observed for **2a**,**b** with a height around 3.0 nm in both cases.

Spectroscopic Characterization of the *n*/*p*-Material. After studying the self-assembly properties of these three small molecules separately, we prepared the hybrid materials by combining *p*-type exTTF fibers (**1**) and *n*-type PBI fibers (**2a**,**b**) by utilizing the electrostatic interactions between negative carboxylic groups (**1**) and positive guanidinium (**2a**) or quaternary ammonium (**2b**) groups in aqueous solution.

When equal volumes of dilute aqueous solutions of **1** (1×10^{-4} M, 10 equiv of $NaHCO_3$) and **2a**/**2b** (1×10^{-4} M) were mixed, we observed an immediate formation of red precipitate in solution. The precipitates based on **1** and **2a** or **1** and **2b** were separated from the starting materials by repeated centrifugation and redispersion in distilled water. The purified homogeneous dispersions of **1** and **2a** and **1** and **2b** in water were characterized by UV−visible absorption spectroscopy (Figures 2a and S3). It is important to note that, the UV−visible spectra obtained for the dispersions were essentially a combination of those acquired for **1** and **2a**/**2b** individually in aqueous solution, indicating that, electronic properties of individually aggregated chromophores (exTTF and PBI) were not perturbed in the co-assembled state. Also intensity in the observed absorption spectra of co-assembly resembles the simulated spectra for the combination of 2:1 equiv of **1** and **2a**/**2b**, which indicates the quantitative electrostatic interactions and formations of co-assembled $\mathbf{1}_2\mathbf{2a}$ and $\mathbf{1}_2\mathbf{2b}$. Moreover, only by addition of polar protic organic solvents such as methanol, the original absorption bands for isolated molecules of **1** and **2a**/**2b** were recovered, disrupting every possible non-covalent interactions in the *n*/*p*-nanostructure. This fact, in turn, attests the reversibility of the process (Figure S4).

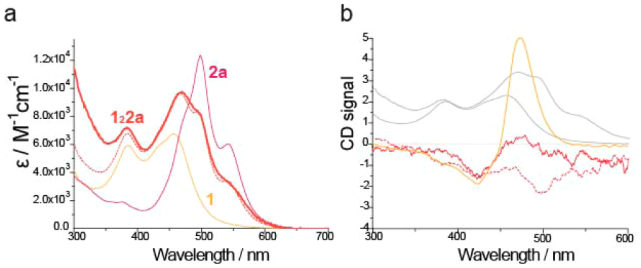

Figure 2. (a) Absorption spectra for aqueous solutions of **1** (yellow) and **2a** (purple) and for the dispersion obtained by mixing of both solutions (solid red). Dashed red line represents the simulated spectra for mixture with a stoichiometry of $\mathbf{1}_2\mathbf{2a}$. (b) Circular dichroic spectra of **1** (yellow), $\mathbf{1}_2\mathbf{2a}$ (solid red), and $\mathbf{1}_2\mathbf{2b}$ (dashed red).

The *n*/*p*-co-assembly of **1** with **2a**/**2b** through electrostatic interactions were also monitored by circular dichroism (CD) spectroscopy. The evolution of the dichroic signal from **1** to $\mathbf{1}_2\mathbf{2a}$ and $\mathbf{1}_2\mathbf{2b}$ is shown in Figure 2b. Initially, as it has been described in our previous work,[7] a soft basic aqueous solution of compound **1**, where the *p*-type exTTF nanofiber were formed, exhibited a strong bisignate signal with a positive Cotton effect at 480 nm, a negative Cotton effect at 431 nm, and a zero crossing point at 456 nm due to the chiral organization of exTTF units. When the dichroic spectra of a clean dispersion of $\mathbf{1}_2\mathbf{2a}$ and $\mathbf{1}_2\mathbf{2b}$ is monitored, it is remarkable that the negative Cotton effect of exTTF at 431 nm is maintained, and two new negative Cotton signals appeared at 542 and 500 nm, which are matching with the absorption bands of **2a**,**b**, being more evident in the case of $\mathbf{1}_2\mathbf{2b}$. These observations indicate the existence of chiral PBIs aggregates in the *n*/*p*-co-assembly which is induced by the exTTF arrays. The positive peak at 480 nm was significantly reduced since it has been presumably neutralized by the intensity of new negative dichroic signals. It is worth to mention that intensity before and

DOI: 10.1021/ja510946c
J. Am. Chem. Soc. 2015, 137, 893−897

after addition of **2a** or **2b** was not comparable due to the scattering in the dispersion of *n*/*p*-co-assembly. Moreover, the characteristic *β*-sheet fingerprint for *p*-type nanofibers of **1** (between 220 and 260 nm) was preserved in the *n*/*p*-nanostructure (Figure S5). All these experimental findings demonstrated the maintenance of the chirality and the order in the co-assembled systems.

The efficient electrostatic interactions between the carboxylate and guanidinium or quaternized amine were confirmed by X-ray photoelectron spectroscopy (XPS) and Fourier transform infrared spectroscopy (FTIR).[6a,9] In XPS measurement, no detectable signals of Na-1s as countercation and Cl-2p and I-3d as counteranions were observed in the 1072, 198, and 620 eV regions, respectively, which indicates that interactions occur between carboxylate and guanidinium or quaternized amine (Figure S6). Moreover, FTIR data of $\mathbf{1}_2$**2a** and $\mathbf{1}_2$**2b** show a complex spectrum in the region 1800−1400 cm^{-1} due to the presence of several bands, stemming from the different carbonyl groups present in the respective complexes. However, a remarkable shift (80−100 cm^{-1}) on the carboxylate band comparing to that band in compound **1** is observed. This fact corroborates that the interaction between both supramolecular systems occurs through the carboxylate and guanidinium/quaternary ammonium ions (Figure S7).

In order to confirm the molecular composition of the materials in $\mathbf{1}_2$**2a** and $\mathbf{1}_2$**2b**, the corresponding thin films were investigated by XPS (Figure S6), which ascertained the quantitative coupling between oppositely charged building blocks at the molecular level. As it has been already reported in other cases, through a Gaussian deconvolution of the N-1s signal obtained by XPS, it is possible to determine the populations of electronically distinct N atoms.[6a] For example, in the case of $\mathbf{1}_2$**2b**, deconvolution of the total N-1s signal intensity revealed the presence of 15% of the oscillator strength derives from the quaternized amine at 403 eV and 85% from the tertiary amines at 400 eV, which were attributed to a 2:1 stoichiometry for the *n*/*p*-co-assembled nanostructure ($\mathbf{1}_2$**2b**).

Microscopy and X-ray Diffraction Studies. The most interesting features of these *n*/*p*-materials were obtained from scanning and transmission electron microscopies (SEM, TEM), and also by small-angle X-ray scattering (SAXS) measurements. Stupp and co-workers thoroughly investigated the co-assembly of small molecules and polymers such as peptide amphiphiles and polysaccharide hyaluronic acids. They reported the formation of ordered sacs and membranes by co-assembly of these molecules.[10] In line with those studies, using the same methodology, we propose the formation of electroactive closed sacs by co-assembly of two self-assembled small molecules (**1** and **2a**/**2b**). These supramolecular ensembles can be easily prepared by injecting small amount of concentrated aqueous solution (5×10^{-3} M) of one chromophore into equally concentrated bulk solution of other (Figure S8). Although these sacs are formed instantaneously, they were allowed to grow further within the solution for several days before investigating the morphology and achieve the maximum organization. SEM of dried sacs revealed the presence of regions with seemingly perfect parallel alignment of fibers, together with randomly distributed fiber areas. In both cases, homogeneous fibers with diameters ranging from 10 to 20 nm were observed. The length of the fibers found to be several tens of micrometers (Figures 3a,b and S9). Moreover, it is possible to observe a dense packing of the fibers longitudinal to its long axis, with a thickness of around 30 *μ*m. To the best of our knowledge, this is the first example where the ionic co-assembly of two oppositely charged self-assembled molecular aggregates leads to the formation of *n*/*p*-type functional material with this level of organization. Moreover, it is important to remark that our approach leads to fibers alignment through the long-axis, which should impact on the charge transport properties of the *n*/*p*-materials, as it has been recently reported by Sakakibara et al.[11]

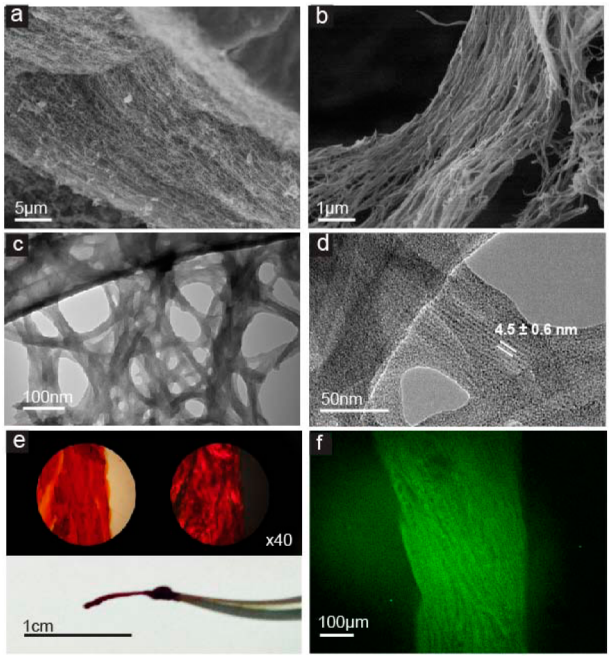

Figure 3. Microscopic images of the co-assembled $\mathbf{1}_2$**2a**. (a,b) SEM micrographs of the fiber-composed membrane at different magnifications. (c,d) TEM micrographs of the fiber-like structures with aligned internal domains at different magnifications (dark regions in the micrograph indicates the positive staining of carboxylates by uranyl acetate). (e) Optical micrograph of a filament without (top left) and with (top right) polarized light, and image of the just-formed filament (bottom). (f) Fluorescence confocal micrograph of the filament.

We further investigated the surface morphology of the *n*/*p*-co-assembled materials by AFM. The AFM images revealed the presence of fibers with a height in the range of 8−14 nm, measured on the most individualized ones (Figure S10), which are in accordance with the diameter observed in SEM images. These results confirm the dramatic increase in overall width of the *n*/*p*-co-assembled materials when compared with the individually self-assembled *p*-type exTTF or *n*-type PBI fibers.

The internal structure of these self-assembled materials was elucidated by TEM and High Resolution-TEM (HR-TEM), by drop-casting a clear dispersion of $\mathbf{1}_2$**2a** or $\mathbf{1}_2$**2b**. Regularly alternating domains arranged longitudinal to the long axes of the fibers were found, as shown in Figure 3c,d (dark regions in the micrograph indicate positive staining of carboxylates by uranyl acetate), with a domain width of around 4.5 ± 0.6 nm (For more TEM and HR-TEM images, please see Figures S11 and S12.)

Interestingly, we found that not only sacs with ordered membranes but also macroscopically aligned bundled filaments can be prepared by manual drawing of one solution into the other using a pipet (Figures 3e and S13). When these filaments are taken out of the solution and deposited on a surface, birefringence was observed along the length of the strand using

DOI: 10.1021/ja510946c
J. Am. Chem. Soc. 2015, 137, 893−897

a polarized optical microscope. This observation also proved the control in the macroscopic alignment of these hybrid materials extending over centimeters. Furthermore, this fact was confirmed by fluorescence confocal microscopy where fluorescence coming from PBI moieties presents an unambiguous orientation along the string axis (Figures 3f and S14).

To verify the extent of supramolecular order in the *n*/*p*-co-assembled material, we carried out the SAXS studies of aligned bundled filaments. The SAXS analysis for $\mathbf{1}_2\mathbf{2a}$ and $\mathbf{1}_2\mathbf{2b}$ showed two peaks with *d*-spacing of 9.3 and 5.8 nm, which were attributed to the (10) and (01) reflections of a rectangular packing, corroborating the presence of long-range order in the hybrid materials (Figure 4). Moreover, X-ray powder diffraction

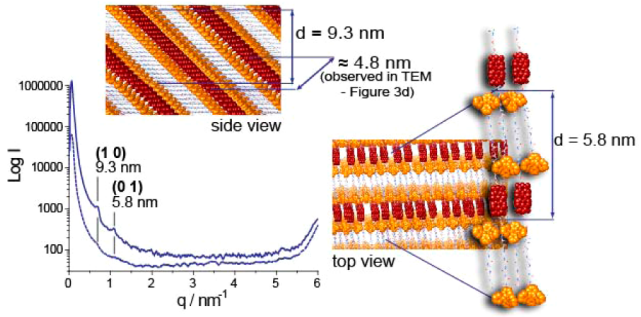

Figure 4. SAXS pattern for the co-assembled filament of $\mathbf{1}_2\mathbf{2a}$ (solid blue) and $\mathbf{1}_2\mathbf{2b}$ (dashed blue) and schematic representation of the organization punctuating the repetition distance. Yellow- and red-colored parts represent the exTTF and PBI units, respectively.

(XRD) experiments supported the existence of well-defined *β*-sheets showing a set of two broad peaks with $2\theta = 9.7°$ and 19.3° (*d*-spacing = 9.1 and 4.6 Å, respectively) (Figure S15). The molecular modeling supports the periodicity in the internal organization which was observed in TEM images with a width of around 3.9−5.1 nm (Figure 3d). A schematic representation the co-assembly is depicted in Figure 4.

Charge Carrier Mobilites. Based on the confined H-aggregate stacking structure of PBI and exTTF motifs with interplanar distances of ∼3.5 Å,[7a,12] presumed value of electron and hole mobilities along the stacking axes were examined by Flash-Photolysis Time-Resolved Microwave Conductivity measurements.[13] Upon photoexcitation with a 355 nm laser pulse at room temperature, films of these composites on quartz substrates displayed fairly clear photoconductivity transients ($\phi\Sigma\mu$), where ϕ and $\Sigma\mu$ denotes the quantum yield of charge-carrier generation and the sum of the charge carrier mobilities, respectively. In contrast to the pristine solid films of **1**, **2a** and **2b** (Figure S16), the co-assembled materials $\mathbf{1}_2\mathbf{2a}$ and $\mathbf{1}_2\mathbf{2b}$ showed an effective photo charge carrier generation with long lifetimes (>3 μs), which suggest that the exciton formed at the *p*/*n* heterojunction were charge separated and freely transferred along the π-stack of **1** and **2a**,**b** (Figures 5a and S17a). The maximum values of the transients $(\phi\Sigma\mu)_{max}$ for $\mathbf{1}_2\mathbf{2a}$ and $\mathbf{1}_2\mathbf{2b}$ were recorded as 5.1×10^{-4} and 1.2×10^{-4} cm^2 V^{-1} s^{-1} respectively, which were one order of magnitude higher than the values recorded for the individual self-assembly of **1** (cations on exTTF units) and **2a** or **2b** (anions on PBI moieties). The observed $(\phi\Sigma\mu)_{max}$ values for **1**, **2a** and **2b** are 4.9×10^{-5}, 2.6×10^{-5} and 6.5×10^{-5} cm^2 V^{-1} s^{-1}, respectively. This implies the existence of highly conducting pathways for holes or electrons in the co-assembly of exTTF and PBI

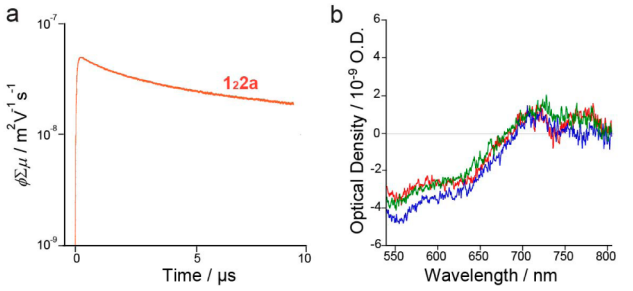

Figure 5. (a) Conductivity transients observed for $\mathbf{1}_2\mathbf{2a}$ upon exposure for 355 nm, 9.1×10^{15} photons/cm^2. (b) Transient absorption spectra recorded for $\mathbf{1}_2\mathbf{2a}$ in solid films upon excitation at 355 nm, 5.5×10^{16} photons/cm^2. The red, green, and blue spectra were recorded immediately after the pulse exposure of **1** (red), **2** (green), and **8** (blue), respectively.

systems. No significant changes in the lifetime of $\mathbf{1}_2\mathbf{2a}$ and $\mathbf{1}_2\mathbf{2b}$ was observed, which indicates that the contribution from terminal groups and counterions are negligible in the charge recombination processes. Linearity in the reciprocal conductivity transients (Figure S18) suggests that the recombination processes in $\mathbf{1}_2\mathbf{2a}$ and $\mathbf{1}_2\mathbf{2b}$ can be interpreted by the second-order protocols. The contribution of negative charge (electron) conductivity in the transient was also confirmed by the selective scavenging of photogenerated electrons in the media (Figure S19), where the decrease of end-of-pulse conductivity (<100 ns range) was observed, associated with a significant elongation of the lifetime of the charge carriers with the long-lived tail (>μs range). Suppressed charge recombination reaction is responsible for the stable positive charge carrier species in the present system. The yield of photocarrier generation was also discussed quantitatively by tracing radical anions of PBI motifs as an indicator (Figure S20). Figures 5b and S17b show the transient absorption spectra for $\mathbf{1}_2\mathbf{2a}$ and $\mathbf{1}_2\mathbf{2b}$, respectively in solid films which were identical to the FP-TRMC results, this providing a clear signature of $PBI^{\bullet-}$ at 780 nm. Based on the molar extinction coefficient of $PBI^{\bullet-}$ (7.4×10^4 mol^{-1}dm^{3}cm^{-1}),[14] the yield of the photocarrier generation (ϕ) was estimated immediately after the pulse exposure and are found to be 2.2×10^{-4} and 1.2×10^{-4} for $\mathbf{1}_2\mathbf{2a}$ and $\mathbf{1}_2\mathbf{2b}$, respectively. On the assumption of balanced number of charges between exTTF cations and PDI anions, the quantitative analysis of ϕ was performed, giving $\Sigma\mu$ in hydrogels of $\mathbf{1}_2\mathbf{2a}$ and $\mathbf{1}_2\mathbf{2b}$ as 0.5 and 0.8 cm^2 V^{-1} s^{-1}, and this is the case giving a high value of $(\phi\Sigma\mu)_{max}$, hence provided the effective heterojunction structures in $\mathbf{1}_2\mathbf{2a}$ and $\mathbf{1}_2\mathbf{2b}$. On the basis of fiber-like structure of the co-assembled $\mathbf{1}_2\mathbf{2a}$ and $\mathbf{1}_2\mathbf{2b}$, anistropic conduction of the charge carriers was also demonstrated for the macroscopically aligned $\mathbf{1}_2\mathbf{2a}$ and $\mathbf{1}_2\mathbf{2b}$ films by rubbing protocols. The conductivity transients depend on the direction of the rubbing (Figure S19), suggesting the presence conductive pathways along the axes of the assembled structures. The relatively low anisotropic ratio of the conductivity transients (1.3 and 1.4 for $\mathbf{1}_2\mathbf{2a}$ and $\mathbf{1}_2\mathbf{2b}$, respectively) is almost consistent to the optical dichroic ratio (1.3 and 1.2 for $\mathbf{1}_2\mathbf{2a}$ and $\mathbf{1}_2\mathbf{2b}$, Figure S21), and there is more room to improve the anisotropic conductivity by the precise control of the orientation of the fibers.

■ CONCLUSION

In summary, we have demonstrated the formation of highly ordered functional materials from small molecules such as π-

DOI: 10.1021/ja510946c
J. Am. Chem. Soc. 2015, 137, 893−897

extended tetrathiafulvalene (exTTF) as electron-donor and perylene-bisimide (PBI) as electron-acceptor, endowed with complementary groups, namely carboxylic acid and guanidinium or quaternary ammonium. The electrostatic co-assembly of two complementary self-assembling nanofibers gives rise to a controlled alignment of the *n*/*p*-material with remarkably high values of photoconductivity. This ease and readily available methodology paves the way to new highly ordered materials with a defined D/A stoichiometry and excellent photoconductivity properties.

■ ASSOCIATED CONTENT

Supporting Information

Details of synthesis and fully characterization by NMR, mass spectrometry, IR, absorption, and CD spectroscopy, SEM and TEM, XRD, and transient photoconductivity measurements. This material is available free of charge via the Internet at http://pubs.acs.org.

■ AUTHOR INFORMATION

Corresponding Author

nazmar@ucm.es

Author Contributions

[⊥]J.L.-A., M.J.R., and C.A. contributed equally to this work.

Notes

The authors declare no competing financial interest.

■ ACKNOWLEDGMENTS

This work was supported by the European Research Council ERC-2012-ADG_20120216 (Chirallcarbon), Ministerio de Economía y Competitividad (MINECO) of Spain (project CTQ2011-24652; BFU2011-29038 to J.L.C; Ramón y Cajal granted to C.A.), and the CAM (FOTOCARBON project S2013/ MIT-2841). N.M. thanks the Alexander von Humboldt Foundation.

■ REFERENCES

(1) (a) Bakulin, A.; Rao, A.; Pavelyev; van Loosdrecht, P. H. M.; Pshenichnikov, M. S.; Niedzialek, D.; Cornil, J.; Beljonne, D.; Friend, R. H. *Science* **2012**, *335*, 1340−1344. (b) Mann, S. *Nat. Mater.* **2009**, *8*, 781−792.

(2) (a) Che, Y.; Huang, H.; Xu, M.; Zhang, Ch.; Bunes, B. R.; Yang, X.; Zang, L. *J. Am. Chem. Soc.* **2011**, *133*, 1087−1091. (b) Kira, A.; Umeyama, T.; Matano, Y.; Yoshida, K.; Isoda, S.; Park, J. K.; Kim, D.; Imahori, H. *J. Am. Chem. Soc.* **2009**, *131*, 3198−3200. (c) Yamamoto, Y.; Fukushima, T.; Suna, Y.; Ishii, N.; Saeki, A.; Seki, S.; Tagawa, S.; Taniguchi, M.; Kawai, T.; Aida, T. *Science* **2006**, *314*, 1761−1764. (d) Röger, C.; Müller, M. G.; Lysetska, M.; Miloslavina, Y.; Holzwarth, A. R.; Würthner, F. *J. Am. Chem. Soc.* **2006**, *128*, 6542−6543.

(3) (a) Hizume, Y.; Tashiro, K.; Charvet, R.; Yamamoto, Y.; Saeki, A.; Seki, S.; Aida, T. *J. Am. Chem. Soc.* **2010**, *132*, 6628−6629. (b) Charvet, R.; Acharya, S.; Hill, J. P.; Akada, M.; Liao, M.; Seki, S.; Honsho, Y.; Saeki, A.; Ariga, K. *J. Am. Chem. Soc.* **2009**, *131*, 18030−18031.

(4) (a) Umeyama, T.; Tezuka, N.; Kawashima, F.; Seki, S.; Matano, Y.; Nakao, Y.; Shishido, T.; Nishi, M.; Hirao, K.; Lehtivuori, H.; Tkachencko, N. V.; Lemmetyinen, H.; Imahori, H. *Angew. Chem., Int. Ed.* **2011**, *50*, 4615−4619. (b) He, Y.; Yamamoto, Y.; Jin, W.; Fukushima, T.; Saeki, A.; Seki, S.; Ishii, N.; Aida, T. *Adv. Mater.* **2010**, *22*, 829−832. (c) Yamamoto, Y.; Zhang, G.; Jin, W.; Fukushima, T.; Ishii, N.; Saeki, A.; Seki, S.; Tagawa, S.; Minari, T.; Tsukagoshi, K.; Aida, T. *Proc. Natl. Acad. Sci. U.S.A.* **2009**, *106*, 21051−21056. (d) Yamamoto, Y.; Fukushima, T.; Saeki, A.; Seki, S.; Tagawa, S.; Ishii, N.; Aida, T. *J. Am. Chem. Soc.* **2007**, *129*, 9276−9277.

(5) (a) Vergara, J.; Barberá, J.; Serrano, J. L.; Ros, M. B.; Sebastián, N.; Fuenta, R.; López, D. O.; Fernández, G.; Sánchez, L.; Martín, N. *Angew. Chem., Int. Ed.* **2011**, *50*, 12523−12528. (b) Hironobu, Hayashi; Wataru, N.; Umeyama, T.; Matano, Y.; Seki, S.; Shimizu, Y.; Imahori, H. *J. Am. Chem. Soc.* **2011**, *133*, 10736−10739. (c) Tasios, N.; Grigoriadis, C.; Hansen, M. R.; Wonneberger, H.; Li, C.; Spiess, H. W.; Müllen, K.; Floudas, G. *J. Am. Chem. Soc.* **2010**, *132*, 7478−7487.

(6) (a) Olivier, J.-H.; Deria, P.; Park, J.; Kumbhar, A.; Andrian-Albescu, M.; Therien, M. J. *Angew. Chem., Int. Ed.* **2013**, *52*, 13080−13085. (b) Faul, C. F. J.; Antonietti, M. *Adv. Mater.* **2003**, *15*, 673−687.

(7) (a) López-Andarias, J.; López, J. L.; Atienza, C.; Brunetti, F. G.; Romero-Nieto, C.; Guldi, D. M.; Martín, N. *Nat. Commun.* **2014**, DOI: 10.1038/ncomms4763. (b) López, J. L.; Atienza, C.; Insuasty, A.; López-Andarias, J.; Romero-Nieto, C.; Guldi, D. M.; Martín, N. *Angew. Chem., Int. Ed.* **2012**, *51*, 3857−3861.

(8) (a) Ghosh, S.; Li, X.-Q.; Stepanenko, V.; Würthner, F. *Chem.—Eur. J.* **2008**, *14*, 11343−11357. (b) Chen, Z.; Stepanenko, V.; Dehm, V.; Prins, P.; Siebbeles, L. D. A.; Seibt, J.; Marquetand, P.; Engel, V.; Würthner, F. *Chem.—Eur. J.* **2007**, *13*, 436−449. (c) Würthner, F.; Chen, Z.; Dehm, V.; Stepanenko, V. *Chem. Commun.* **2006**, 1188−1190. (d) Li, X.-Q.; Stepanenko, V.; Chen, Z.; Prins, P.; Siebbeles, L. D. A.; Würthner, F. *Chem. Commun.* **2006**, 3871−3873.

(9) Kamino, A.; Koyano, H.; Ariga, K.; Kunitake, T. *Bull. Chem. Soc. Jpn.* **1998**, *69*, 3619−3631.

(10) (a) Wall, B. D.; Diegilmann, S. R.; Zhang, S.; Dawidczyk, T. J.; Wilson, W. L.; Katz, H. E.; Mao, H. Q.; Tovar, J. D. *Adv. Mater.* **2011**, *23*, 5009−5014. (b) Zhang, S. M.; Greenfield, M. A.; Mata, A.; Palmer, L. C.; Bitton, R.; Mantei, J. R.; Aparicio, C.; de la Cruz, M. O.; Stupp, S. I. *Nat. Mater.* **2010**, *9*, 594−601. (c) Capito, R. M.; Azevedo, H. S.; Velichko, Y. S.; Mata, A.; Stupp, S. I. *Science* **2008**, 812−816.

(11) Sakakibara, K.; Chithra, P.; Das, B.; Mori, T.; Akada, M.; Labuta, J.; Tsuruoka, T.; Maji, S.; Furumi, S.; Shrestha, L. K.; Hill, J. P.; Acharya, S.; Ariga, K.; Ajayaghosh, A. *J. Am. Chem. Soc.* **2014**, *136*, 8548−8551.

(12) (a) Percec, V.; Sun, H. J.; Leowanawat, P.; Peterca, M.; Graf, R.; Spiess, H. W.; Zeng, X.; Ungar, G.; Heiney, P. A. *J. Am. Chem. Soc.* **2013**, *135*, 4129−4148. (b) Chen, Z.; Baumeister, U.; Tschierske, C.; Würthner, F. *Chem.—Eur. J.* **2007**, *13*, 450−465.

(13) (a) Saeki, A.; Koizumi, Y.; Aida, T.; Seki, S. *Acc. Chem. Res.* **2012**, *45*, 1193−1202. (b) Acharya, A.; Seki, S.; Saeki, A.; Koizumi, Y.; Tagawa, S. *Chem. Phys. Lett.* **2005**, *404*, 356−360. (c) Seki, S.; Koizumi, Y.; Kawaguchi, T.; Habara, H.; Tagawa, S. *J. Am. Chem. Soc.* **2004**, *126*, 3521−3528.

(14) (a) Seki, S.; Saeki, A.; Sakurai, T.; Sakamaki, D. *Phys. Chem. Chem. Phys.* **2014**, *16*, 11093−11113. (b) Saeki, A.; Tsuji, M.; Seki, S. *Adv. Energy Mater.* **2011**, *1*, 661−669.

DOI: 10.1021/ja510946c
J. Am. Chem. Soc. 2015, 137, 893−897